This device is provided with a screw auger. Maximum rotation of the auger is 35 rpm and its ascent and descent speed is 0.005 m/sec and drifting speed is 0.005 m/sec. In this test, for the excavation, this auger is replaced by excavating blade of 0.2 m width. It could move up, down, left and right directions. Also, movement of blade in a horizontal direction makes it possible to shift away the excavated material smoothly from the slope. All the processes of excavation are controlled by 4 stepping motors. This in-flight excavator could be controlled manually or in semi-automatic way from the operating room.

3 DETAILS OF CENTRIFUGE MODEL TESTS

Bulk unit weight (γ_t) and w for each test case of Narita sand and Kanto loam are shown in Tables 2 and 3, respectively. Experiments carried out for Narita sand and Kanto loam are mainly explained here. For both of these soils, one normal excavation and 3 combined excavations (normal + toe) were performed. One normal excavation test for mixed soil ($\gamma_t = 14.94$ kN/m^3, w = 9.65%) was also performed to compare the image analysis results of three types of soils during normal excavation failure.

Table 2. Experimental conditions for Narita sand.

Type of excavation cases	Normal R-8-B-0	Combined R-2-B-5	Combined R-4-B-3	Combined R-6-B-2
γ_t (kN/m^3)	10.94	12.56	12.18	12.70
w (%)	9.89	10.75	9.22	9.22
Centrifuge acceleration	31.3	31.3	31.6	31.8
Failure height (Row) (m)	2.985	0.746	1.507	2.275
Failure depth (Bottom) (m)	0	1.565	0.948	0.636
Real height at failure (m)	2.985	2.311	2.455	2.911
$H_{cr} = \{(4*c)/\gamma_t\}$(m)	3.576	3.115	3.211	3.079

Table 3. Experimental conditions for Kanto loam.

Type of excavation cases	Normal R-7-B-0	Combined R-2-B-4	Combined R-4-B-2	Combined R-6-B-1
γ_t (kN/m^3)	8.93	9.00	9.02	8.95
w (%)	91.68	91.11	90.17	88.16
Centrifuge acceleration	31.8	31.3	31.3	31.8
Failure height (Row) (m)	2.65	0.746	1.493	2.275
Failure depth (Bottom) (m)	0	1.252	0.626	0.318
Real height at failure (m)	2.65	1.998	2.119	2.593
$H_{cr} = \{(4*c)/\gamma_t\}$(m)	2.742	2.721	2.119	2.593

Each excavation (cut) was carried out vertically downward and outward. In case of normal excavation, cutting was started from the slope surface to vertically downward and up to toe level. Width of each vertical cut of the model slope in normal excavation is 0.01 m. Each vertical cut (above the toe level) is represented by "Row (R)" and it is followed by the numbers as follows; R-1, R-2, R-3 and so on. R-1 represents the 1st cut, excavating at 0.01 m distance from the toe of the model slope. Similarly, R-2 and R-3 represent the second and third cuts, excavating the model slope at 0.02 and 0.03 m distances from the model slope toe, respectively. Combined excavation represents the trench excavation at particular normal cut (row). Trench excavation represents the vertical cut behind and below the toe level at particular R. Depth of each cut of trench of model is fixed at 0.01 m and trench excavation is represented by "Bottom (B)" which is followed by numbers as follows; B-1, B-2, B-3, and so on. B-1 represents the cut at 0.01 m below from the toe level. Similarly, B-2 and B-3 represent the cuts at 0.02 and 0.03 m depths from the model slope toe level, respectively.

Particular excavation might be either normal excavation or the combination of normal and trench excavations. Therefore, each case of excavation shown in Tables 2 and 3 is represented by the combination of normal (Row) and trench (Bottom) cuts. For example: R-2-B-5. This represents the width of normal cut behind and at the toe level is 0.02 m (i.e., at 0.02 m distance from the model slope toe) and depth of trench cut behind and below the toe level is 0.05 m; showing the excavation at 0.02 m distance from the toe and up to 0.05 m depth below the toe level. Similarly, R-8-B-0 represents the 8 cuts of "Rows", i.e., at 0.08 m distance from the toe. Here, B = 0 represents the excavation made without any trench excavations, i.e., only normal excavation.

In case of combined excavation, at first normal excavation was followed. Once the normal excavation reached the predetermined distance from the toe, trench excavation was followed. As mentioned earlier, depth of each bottom cut of trench excavation is 0.01 m. Two minutes interval was allowed after each bottom cut. Trench excavation was continued till the slope was failed. In Tables 2 and 3, excavation cases are named after the position of excavation where the slopes were failed.

In all the soil types, at first, normal excavation was carried out by cutting the slope behind the toe

in rows, until the slope was failed. In this type of excavation, cutting blade of excavator was vertically moved down from the slope surface and then moved outward horizontally when the blade reached the toe level of that cut. Two minutes interval time was allowed between each cut. Slope of Narita sand was failed at R-8-B-0. For Kanto loam and mixed soil, failure occurred at R-7-B-0. Combined excavation was carried at certain intervals within the distance of failure of normal excavation. Here, R-2, R-4 and R-6 were chosen to carry out the combined excavation.

In this research, height of the slope in the field from the toe level was assumed to be 5 m. In the model, height of the slope from the bottom of the model was 0.26 m and the height of the slope from the toe level was made 0.16 m. To make the slope height of 5 m, centrifuge acceleration was increased up to 31.3G. Similarly, for other cases also acceleration was fixed in such a way that the real height of the slope in the field becomes 5 m. Accelerations for each case are shown in Tables 2 and 3. During the centrifuge test, acceleration was increased gradually in steps from 5~10~15~20~25~31.3G. Once the vertical displacement become constant at 31.3G, then the excavation process was started.

4 TEST RESULTS AND DISCUSSIONS

Excavation test results of Narita sand and Kanto loam are mainly discussed here. Critical failure height for each case of excavation failure is shown in Tables 2 and 3. In the table, all the values are changed into real field value by multiplying the data obtained from model test by the respective centrifuge acceleration values. "Failure height" in tables represents the height of slope above the toe level just before the failure. Similarly, "failure depth" represents the depth of trench cut below the toe level. "Critical failure height" is the summation of failure height and failure depth. "Critical height (H_{cr})" shown in the Tables 2 and 3 was calculated theoretically by using the equation where bulk unit weight and cohesion are used. Critical heights calculated theoretically showed higher values than the critical failure height obtained for each test. In both Narita sand and Kanto loam, critical failure height obtained for the normal excavation case are very closer to critical height calculated whereas those obtained for the combined excavation cases, critical failure heights obtained are smaller than the critical heights calculated using the equation. Therefore, one should be careful while calculating the critical failure height during the combined excavation.

Figure 3 shows the failure height (Row) and failure depth (Bottom) just before the failure at particular distances of excavation from the toe. Excavation position (R-cut) of the model tests is multiplied by the

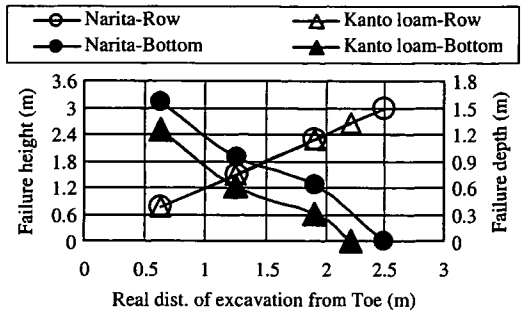

Figure 3. Failure height, failure depth and distance.

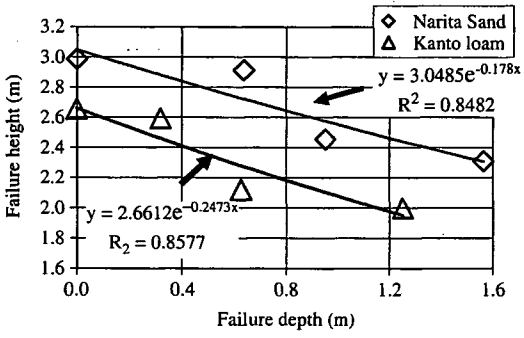

Figure 4. Relationship between failure height and failure depth.

centrifuge acceleration to get the real distance of excavation position from the toe. Non-linear decrease in failure depths with the increase in the real distance of excavation position is seen from the toe. This graph shows the inverse relationship between failure heights and failure depths with the increase in the position of distance of excavation from the toe. A non-linear relationship could be seen in case of failure depth. Graph shown in Figure 4 also shows the relationship between failure height and failure depth. Exponential regression lines shown in the figure could be used for predicting the probable failure height at particular depth of excavation. Figure 5 shows the non-linear relationship between critical failure height and real distance of excavation position just before the failure. From the graph, it could be observed that the critical failure height increases with the increase in the distance of excavation position from the toe. But the increment rate decreases with the increase in the excavation distance from the toe. This implies that at toe or near the toe, if the trench excavation is made, then the failure of slope occurs before it reaches the critical failure height that was obtained from the normal excavation. Henceforth, care should be taken while making the trench excavation.

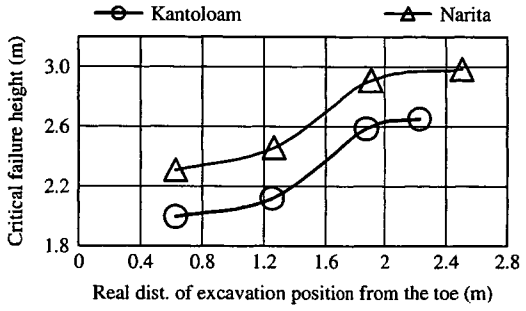

Figure 5. Real height and distance of excavation position from the toe just before the failure.

Decrease in the critical failure height with the increase in the failure depth (trench excavation) might be thought of due to the increase in the overburden pressure (weight of extra height) behind the cut. Generally, when the toe of the slope is excavated, shear strain is accumulated near the toe. With the advancement in the combined excavation steps near the toe, overburden pressure continues to increase. Continuous increment in the overburden pressure behind the cut increases the shearing strain which finally leads to failure and slope gets failed. This is the reason why critical failure height near the toe of the slope is smaller than those at farther distances from the toe. Therefore, for Narita sand and Kanto loam, critical failure height during R-2 cut shows the minimum value in comparison to R-7 and R-8 cuts where the critical failure heights have maximum values. From the results mentioned in Figures 2 to 5, it could be said that the maximum value of critical failure height could only be obtained for normal excavation cases and this critical failure height decreases with the decrease in the distance of excavation position as well as with the increase in the trench excavation depth.

The trend of increment of critical failure heights shown in Figure 5 for Narita sand and Kanto loam are similar. But the critical failure height obtained from the model test for Narita sand is higher than that for Kanto loam. This might be due to the effect of cohesion: Narita sand has higher cohesion value than Kanto loam (Table 1). Here, compaction pressure for Narita sand and Kanto loam were also different; Narita sand being prepared under 50 kPa and Kanto loam being prepared under 25 kPa. Except R-7-B-0 case of Narita Sand, in all the cases of Narita sand and Kanto loam soils, failure was partially occurred within the slope just behind the cut showing very small movement of soil masses behind the cut. But for mixed soil, large failure behind the cut with large movement soil mass in block behind the cut was seen. In order to check the movement of soil masses after the failure, image analysis was carried out from the photographs taken before the start of excavation and after the failure.

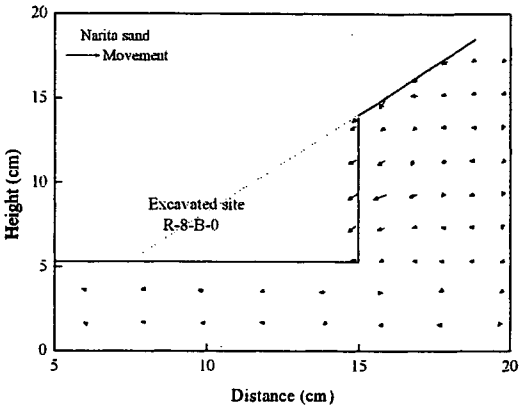

Figure 6. Movement at failure for Narita sand (R-8-B-0).

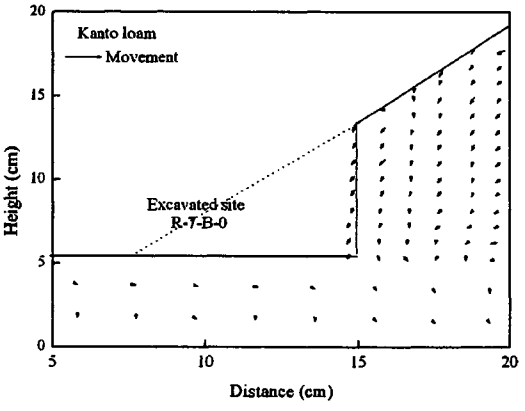

Figure 7. Movement at failure for Kanto loam (R-7-B-0).

Image analysis was done from the lines drawn on the rubber membrane. Figures 6, 7 and 8 show the relative movement of slopes before the start of excavation and just before the failure. It was found that the movement behind the cut before the failure was small for Narita sand and Kanto loam in comparison to mixed soil; mixed soil showing the maximum movement while Kanto loam showing the minimum movement.

Figures 9 and 10 show the vertical displacement measured from LVDTs set up on the top surface of the slope for normal excavation cases of Narita sand and Kanto loam, respectively. Bold vertical lines in the graph represent the steps of excavation. In both the graphs, gradual increase in vertical displacement with the increase in the steps of excavation could be observed. Comparing the amount of vertical displacement of each LVDT (D-1, D-2 and D-5), D-1 shows the maximum value and D-5 shows the minimum. This pattern of gradual decrease in vertical displacement shows the forward and downward movement of

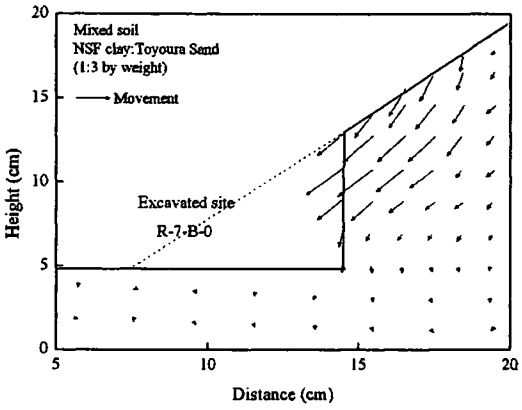

Figure 8. Movement at failure for mixed soil (R-7-B-0).

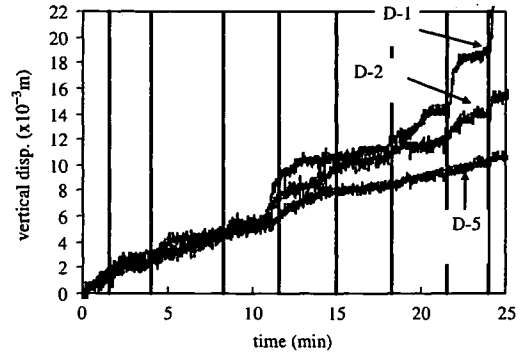

Figure 9. Vertical displacement with time (Narita sand).

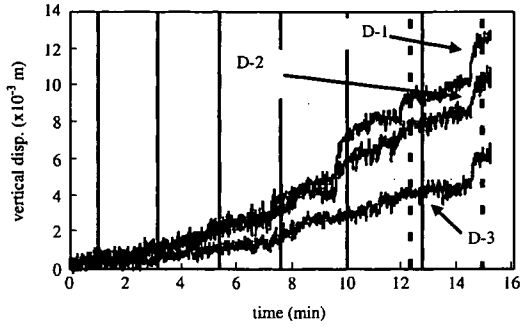

Figure 10. Vertical displacement with time (Kanto loam).

slope with the increase in excavation steps. Sudden increment of displacement just before the failure was seen for the LVDT (D-1) which is at the nearest distance from the slope crest. This sudden increase in the displacement might be useful in predicting the possible failure.

5 CONCLUSIONS

(1) Maximum critical failure height is obtained only for normal excavation. In case of combined excavation, critical failure height (failure height + failure depth) decreases with the increase in the trench excavation depth. Reduction in the critical failure height near and towards the toe is due to the increase in the overburden pressure (weight of extra height) behind the cut.

(2) The trend of increment in critical failure height obtained for both Narita sand and Kanto loam are almost same. But the critical failure height obtained for Narita sand is higher than that obtained for Kanto loam. This might be due to cohesion values or compaction pressure used for preparing the soil.

(3) From the image analysis, failure pattern or the movement of slope behind the cut could be observed. Partial failure and smaller movement behind the cut were seen for Narita sand and Kanto loam. Whereas larger and block movement were seen for mixed soil.

(4) Gradual increment in vertical displacement measured on the top surface of slope showed the forward and downward movement of the slope. Sudden increment in vertical displacement, D-1 near the slope crest is helpful in predicting the failure.

ACKNOWLEDGEMENT

This research is partially carried out under the Health and Labor Sciences Research Grants of Ministry of Health, Labor and Welfare, Japan.

REFERENCES

Japanese Geotechnical Society (JGS0051-2000). Methods of classification of Geomaterials for Engineering Purposes, *Soil testing methods and explanation*: 213–245.

Tamrakar, S. B., Toyosawa, Y., Itoh, K. & Kusakabe, S. 2005. Failure mechanism of slopes in the centrifuge using In-flight excavator, *International symposium on Landslide Hazard in Orogenic Zone from the Himalaya to Island Arc in Asia*, Kathmandu, Nepal, 25–26 September 2005: 255–264.

Toyosawa, Y., Horii, N. & Tamate, S. 1998. Deformation and failure behavior of anchored retaining wall induced by excessive excavation in centrifuge model tests, *Research Reports of the National Institute of Industrial Safety (NIIS-RR-97)*: 35–46.

POSSIBILITY OF MEASUREMENT OF SLOPE MOVEMENT DURING THE SANDY SOIL SLOPE FAILURE IN CENTRIFUGE

Tamrakar Surendra Bahadur, Japan National Institute of Occupational Safety and Health, Tokyo, Japan
Toyosawa Yasuo, Japan National Institute of Occupational Safety and Health, Tokyo, Japan
Tanaka Hiroyuki, Hokkaido University, Hokkaido, Japan
Itoh Kazuya, Japan National Institute of Occupational Safety and Health, Tokyo, Japan

ABSTRACT

Measurement of slope movement during the failure sandy slopes was studied by conducting manual excavations at the lower part of the slope in case of small size full scale tests and by in-flight excavations in case of centrifuge tests until failure occurred. Stepwise and sharp increment of slope movements of slope surface and slope top during and just before the failure with the elapsed time of excavation steps were seen in both the cases. Quick failure was seen for slopes which have higher slope angle and slope height in both the cases. Similar trends in measurement of all the instruments were seen. This showed the possible applicability of tilt sensors in the real field excavations. In centrifuge excavations, large deformation was seen near the slope crest. Limit equilibrium analysis was also carried out.

RÉSUMÉ

La mesure du mouvement de pente pendant la chute des pentes arénacées a été étudiée en conduisant l'excavation manuelle à la partie inférieure de la pente en cas d'essai à grandeur nature de petit modèle et l'excavation en vol en cas d'essai centrifuge. Dans tous les deux cas, l'augmentation par degrés et brusque du mouvement à la surface et au sommet pendant et juste avant la chute a été observée, ainsi que la chute rapide pour les pentes qui ont un angle aigu et une hauteur élevée. On a observé une tendance semblable du changement des angles mesuré par le détecteur d'inclinaison et de la déformation mesurée par le détecteur de laser et le transducteur de déplacement vertical. Ceci a montré l'applicabilité du détecteur d'inclinaison dans un vrai chantier. En cas d'excavation centrifuge, une grande déformation a été observée près de la crête de pente. L'analyse d'équilibre de limite a été également effectuée.

1. INTRODUCTION

Slope failure due to the human induced construction works (excavation, embankment, etc.) sometimes takes the lives of the workers. In Japan, every year around 30 to 40 cases of such accidents are recorded. More than 50% of such accidents take place during the cutting or leveling the trench of lower part of slope. Slopes become safe only when they are excavated up to safe slope angle or some other protective works are carried out. But during excavation, slopes are at higher risk of failure. In many cases, without any prior signals of failure, instantaneous movement of slope occurs and the workers do not find sufficient time to escape and hence, accidents take place. To prevent such accidents, one should understand the failure mechanism. Also, it would be better if one could measure, predict and inform about trend of slope movement just before the failure.

In this research, failure mechanism of sandy slopes is studied by conducting small size full scale tests and centrifuge tests. For this, river sand was used. In case of small scale full size test, three tests were conducted by varying their slope angle from 50, 60 and 70 degrees along with slope heights varying from 1.3 to 2.2m for each slope angle. Manual excavation was made at the lower part of the slope (toe and trench excavations) until the slope get failed. Here, the trend of slope movement (degrees of movement and amount of deformation) were observed by placing tilt sensors and laser sensors on the slope surface and on the slope top, respectively. In case of centrifuge tests, model slopes were prepared by static compaction within the apparatus box and cutting them into required dimensions. In this case also, three slope angles, 50, 60 and 70 degrees were used. They were then run into 6 and 10 time of gravity acceleration to obtain two slope heights. Vertical deformation of the model slope top was measured by linear variable differential transducers (LVDTs). In this case, excavation of lower part (toe and trench) of the model slopes were carried out by using in-flight excavator until failure occurred. Limit equilibrium analysis for the centrifuge model tests were also carried out to compare the failure pattern in the test and in the analysis.

Changes in the slope angle measured by tilt sensor and deformations measured by laser sensors placed on the slope top and slope surface due to excavation in case of small scale full size test showed similar trend. With the possible measurement of slope movement by tilt sensor during and just before the failure showed the possibility of using them in the real excavation field. In case of centrifuge, while comparing the deformation time graph, failure of slope occurred just after the larger deformations of the LVDT's placed near the slope crest, there by showing the most suitable place for deformation measurement. Limit equilibrium analyses were carried out for centrifuge model tests and factor of safety data were compared. Since the factor of safety for all the tests were around 1, it could be

said that centrifuge test results were appropriate.

2. EXPERIMENTS AND EXPERIMENTAL CONDITIONS

2.1 Small Size Full Scale Test and Instrumental Set Up

In order to carry to out the small size full scale test in the laboratory, a full scale test box was made. Framework of the test box is constructed from the wooden planks, which are supported externally by the iron plates/beams. Frameworks shown in Photo 1 are used. Framework has two sections; lower cross section is 1.35m x 2.7m with 1.3m height and upper cross section is 1.35m x 1.2m with 0.9m. For smaller height slopes, only frontal section is used so that the total slope height is almost equal to 1.3m. In this case, weight of material in the upper section behind the slope might affect the failure movement of frontal section. Layout of small height model is shown in Fig. 1(a). For larger slope height, whole the height of the box is used so that the total height of the slope becomes almost equal to 2.2m. Outline of such model is shown in Fig. 1(c). Base of the box (slope) is 0.3m. Hence the slope heights for small and large slopes become 1m and 1.9m.

River sand was used as the test material. Here, medium dense test model was tried to obtain. Manual compaction was done in layers by spreading and tamping the sand with small wooden planks. Once the compaction was over, wooden planks of the front as well as side faces of model box were removed and cutting of slopes were done so that the test model of desired slope angle and slope height could be obtained. With three slope angles (50, 60 and 70 degrees) and two slope heights (1m and 1.2m), in total six tests were conducted. Water content and bulk unit weight of each test are shown in Table 1. Outline of model slopes are shown in Figs. 1(a), (b) and c).

Once the desired slope of the test model was ready, then the set up of measuring instruments was done. Three types of measuring instruments were used; laser sensor, direct vertical displacement transducers (VDTs) and tilt sensor. First two instruments were used to measure the deformation of slope surface and slope top (vertical) where as the third instrument was introduced to measure the change in the angle due to the movement of slope surface and deformation of the slope top due to excavation. Tilt sensor is an acceleration sensor which is made in such a way that its output voltage could be changed into the tilt angle. Tilt sensor used in this research is shown in Photo 2. This could measure the angles in both X and Y directions with possible measurement of positive and negative angles. It's measuring range is ±20° with sensitivity of 100mV/deg. This tilt sensor could also be used a thermo sensor. But this facility was not used in the tests here as tests were conducted inside the laboratory where temperature is considered to be constant.

Photo 1. (a) Lower section and (b) Whole framework

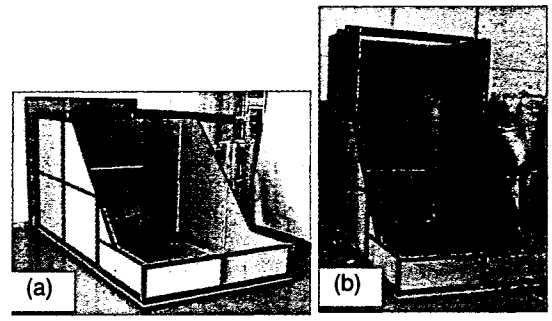

Figure 1. Outline of Small scale full size tests (a) for Slope-I-2, (b) for Slope-IV-1, Slope-V-2 and (c) for Slope-II-3, Slope-IV-2, Slope-V-2

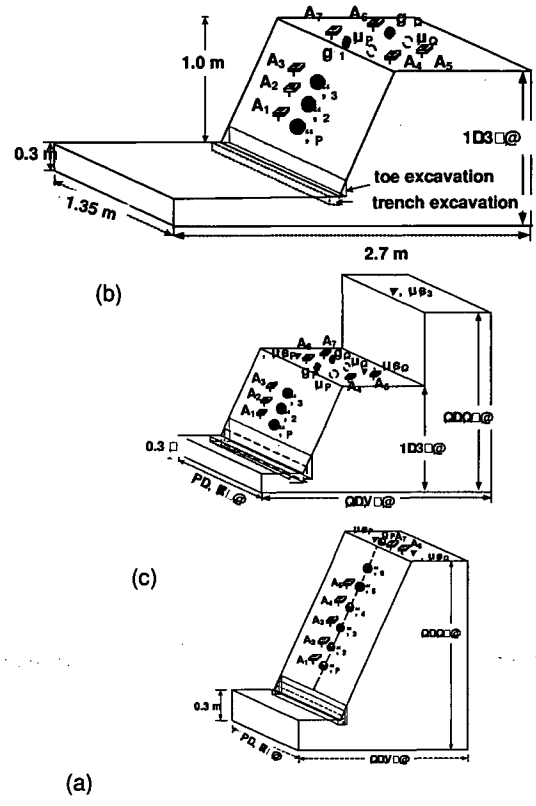

Table 1. Experimental conditions.

Test	Slope Angle	Water Content	Unit Weight	Failure Steps	Failure Time
	°	(%)	kN/m^3		min.
Slope-I-2	50	8.05	13.78	5	33.5
Slope-II-3	50	8.54	14.69	2	6.5
Slope-IV-1	60	7.55	15.30	13	99.6
Slope-IV-2	60	7.55	15.30	8	51 0
Slope-V-1	70	7.00	15.48	21	192
Slope-V-2	70	7.00	15.48	7	46.8

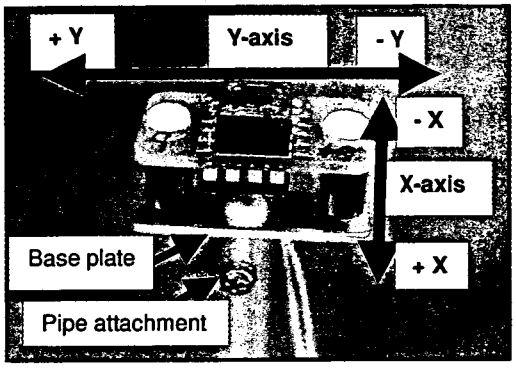

Photo 2. General outline of tilt sensor

Photo 3. Setting up of instruments (Slope-I-2)

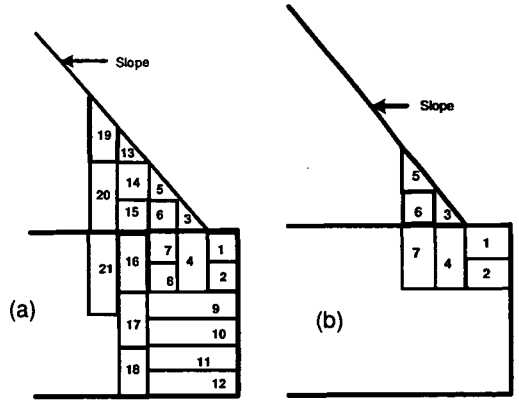

Figure 2. Steps of excavation (a) for Slope-V-1and (b) for Slope-V-2.

Target positions for the laser sensors were set up perpendicularly on the slope surface and slope top. Laser sensor and VDTs were then set up on the required positions. Movement of the slope surface measured by laser sensors is represented by S_1, S_2, S_3, etc. Similarly vertical and horizontal movement of laser sensors set up the slope top are represented by V_1, V_2, and H_1, H_2 respectively. Vertical deformation of VDTs is represented by VDT_1, VDT_2, etc. Tilt sensors were set up both on the slope surface and slope top. They were directly inserted with the tubular pipes attached at the base of the sensor. Tilt sensor placed on the slope surface is represented by A_1, A_2, A_3, etc. and those on the slope top are represented by A_4, A_5, A_6, etc. General outline of instrument set up is shown in Figs. 1(a), (b) and (c) and Photo 3. Tilt-sensors were set up near and on the same line of the laser targets.

Excavation was done manually at the bottom of the slope as shown in Fig. 2. Both toe and trench excavations were done in steps. Depth and width of each trench as well as the toe excavation were different. Between each step of excavation, about 5 minute time interval was allowed so that the movement of slopes as well as the top surface of the slope could be observed. Excavations were continued until the slope was failed. In all the tests, at first, the trench excavation was done. In case of Slope-V-1, total numbers of excavation steps were 21 where complete failure took place. In contrary, total number of steps for Slope-V-2 was 7 by which complete failure took place. Steps and elapsed timing for failure for each test are also shown in Table 1.

2.2 Centrifuge Tests and Instrumental Set Up

NIIS-centrifuge Mark-II (Horii et. al 2006) was used for the test. For the excavation of the centrifuge model slope, in-flight excavator (Toyosawa et. al 1998) was used by changing its auger with excavating blade which is 20 cm in width. Here also, River sand was used. To prepare the model slope, at first soil specimen was statically compacted with in a model box (0.45m x 0.20m x 0.272m), using bellofragm cylinder. Compaction was done under 200 kPa with 15 layers; 3 minutes of compaction time was allowed for each layer. In between each layer, Kaoline power was spread so that failure pattern could be seen clearly during failure of slope.

Once the compaction was completed, model slope ground was trimmed to its required dimension. To reduce the friction between the model sand ground and the wall of the model box, rubber membrane was used and thin film of grease was applied in between rubber membrane and apparatus wall. On the rubber membrane, 1cm X 1cm square boxes were drawn in advance so that excavation width and height could be decided while the test was under centrifuge.

Once the model box was ready, it was shifted to centrifuge platform and four direct contact type linear variable differential transducers (LVDTs) were set up on the slope surface. In-flight excavator was then lowered and set up so that its blade lies well within the model apparatus box and could move freely during the operation. Operation of in-flight excavation was done from the control room. Excavation steps for centrifuge are shown in Fig. 3, where the number represents the steps. Other than 50A, all the test models have same trench depth. As in small scale full size test, here also slopes with three angles 50, 60 and 70

degrees were prepared. Total height of each model slope ground was around 0.25m. Since the thickness of the model base is 0.04m, the height of slope becomes 0.21m. To simulate two types of slope heights as in small scale full size tests, centrifuge tests were conducted in 6g and 10g. During the centrifuge test, centrifuge acceleration was increased in two steps; 0~3~6g or 0~5~10g. Bulk unit weight, slope height, centrifuge acceleration, failure step and failure time for each test are shown in Table 2. General layout of 50, 60 and 70 degree slope models are shown in Fig. 4(a), (b) and (c) respectively. Water content of the tests was varied from 7.3 to 8.11%.

Table 2. Centrifuge model tests conditions

Test	Unit Weight	Slope Height	Centrifuge Acceleration	Failure Step	Time
	kN/m^3	m	ng		min.
50A	14.87	1.24	6	11	11.50
50B	14.96	2.06	10	9	10.49
60A	14.96	1.22	6	10	12.25
60B	14.98	2.06	10	3	3.52
70A	14.98	1.15	6	3	1.39

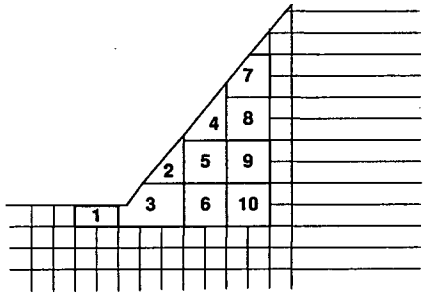

Figure 3. Excavation steps for centrifuge tests

2.3 Limit Equilibrium Analysis and Direct Shear Test

To define the cohesion and angle of shearing values to carry out the limit equilibrium analysis of centrifuge test models, direct shear test was conducted where specimens were prepared by static compaction under 200 kPa. Each specimen was prepared with four-layer compaction; each layer was compacted for 3 minutes. During the test, consolidation was done in four steps; 50, 100, 150 and 200 kPa and consolidation was stopped using 3t-method. Shearing was done at 0.02 mm/min under constant pressure.

Limit equilibrium analysis for each centrifuge test model was conducted using commercially available "Geo-Slope" slope stability analysis software. Dimension of each analysis model is same as that with in the centrifuge test for all the tests except 50A just before the failure. But in the analysis, all the centrifuge dimensions were multiplied by centrifuge acceleration during failure. Automatic determination of failure plane was selected and determined automatically. Factory of safety from the moment equilibrium using Ordinary method, Bishop's method and Morgenstern-Price (M-P) method was compared finally.

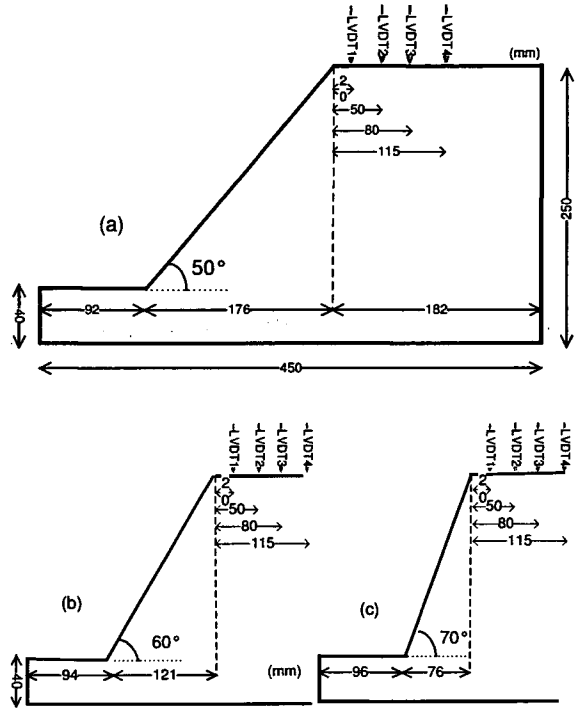

Figure 4. General layout of centrifuge slope models

3. RESULTS AND DISCUSSION

3.1 Small Scale Full Size Test

In the Figs. 5, deformations measured on the slope top of different small scale full size tests are shown. Here, V and VDT represent the vertical deformation measured by laser sensor and vertical displacement transducers. Digits followed by previous letters represent the distance from the slope crest in centimeter. For Slope-II-3 and Slope-IV-2 and Slope-V-2, deformations measured by VDTs are only shown. Comparing the total time taken for short and large slope heights for same slope angle, it could be observed that the total elapsed time for failure is longer for smaller slope heights than that for longer slope heights. Also, comparing the total elapsed time for failure for both slope heights with slope angles varying from 50 to 70 degrees, it was observed that smaller the slope angle, longer the time for failure. In all the test cases, with the increase in the excavation, gradual increment in the deformation was seen. At the beginning, it was difficult of see the clear increments, but just with the increase in excavation portion and elapsed time, large increment was observed. In all the test cases, laser and VDTs nearer to the slope crest showed the maximum and sharp movement just before the

failure. This shows the possible position for the measurement of slope movement during the excavation in order to predict the failure in advance. Movements of slope surface and slope top during the excavation and just before the failure measured by laser sensors for Slope-I-2, Slope-IV-1 and Slope-V-1 are shown in Figs. 6, 7 and 8, respectively. Bold vertical lines in the figures show the trigger for just before and after the excavation. In all the cases, it could be seen that the movement of S_1 was the maximum as it is in the closest distance from the excavation. Others gradually increase. Sharp increment just before the failure is more prominent in both the places (slope surface and slope top). Measurement of tilt angle either on the slope surface or on the slope top or both for Slope-I-2, Slope-IV-1 and Slope-V-1 are shown in Figs. 9(a), (b), 10 and 11(a), (b), (c). Although movements of each sensor for both X and Y directions were measured, here mainly movements along X direction are shown. At the beginning where small excavations were only made, clear increment in tilt angles was not seen. But after certain elapsed time, gradual increment in tilt angle was seen, which sharply increases just before the failure. Comparing the laser sensors data (including VDTs data) of Figs. 5(a), (c), (e) and Figs. 6, 7, 8 and tilt sensors data of Figs. 9, 10, 11, similar trend of movements were observed. This shows the applicability of possible measurement of slope failure pattern so that prediction of failure could be done in advance. In Fig. 11(c), movement of tilt sensors on the slope top along Y direction for Slope-V-1 is shown. Sharp increment before failure was seen. Therefore, knowing the movement along X and Y directions with tilt sensors, possible direction of failure could also be predicted in advance.

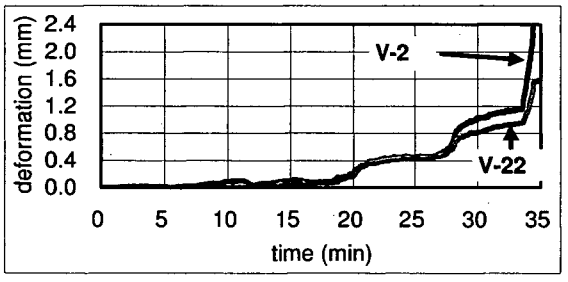

Figure 5(a). Deformation of slope top for Slope-I-2

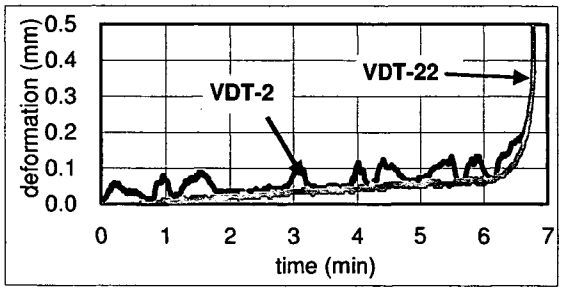

Figure 5(b). Deformation of slope top for Slope-II-3

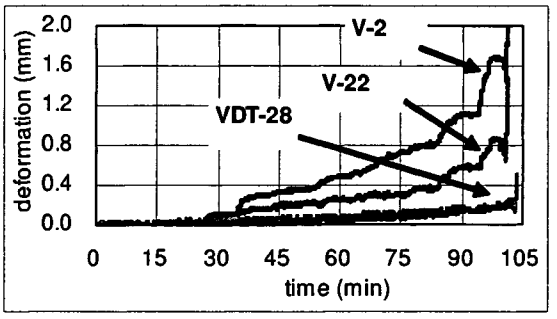

Figure 5(c). Deformation of slope top for Slope-IV-1

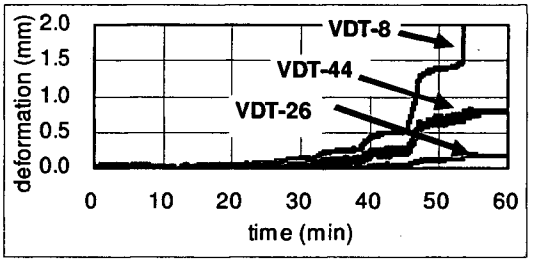

Figure 5(d). Deformation of slope top for Slope-IV-2

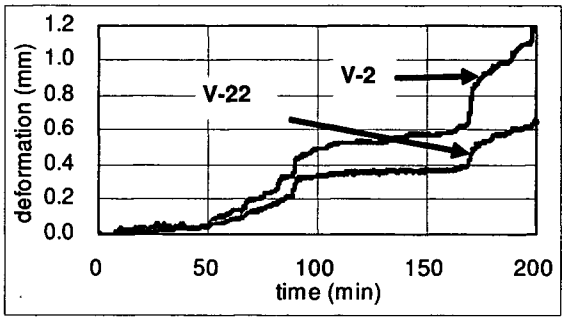

Figure 5(e). Deformation of slope top for Slope-V-1

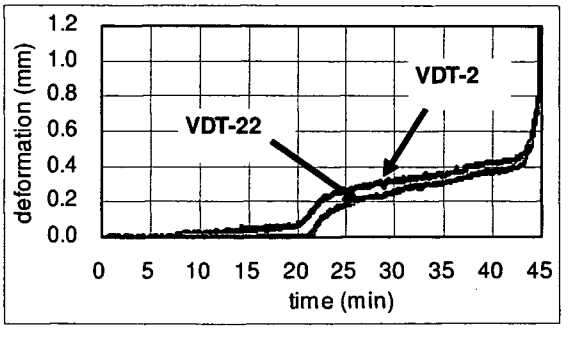

Figure 5(f). Deformation of slope top for Slope-V-2

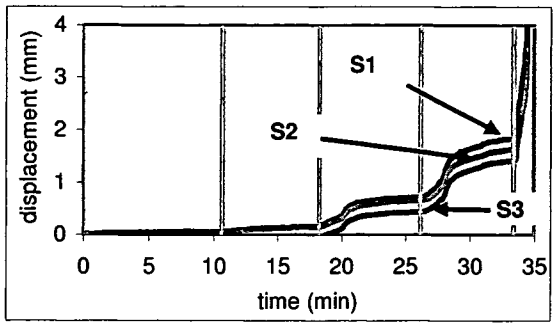

Figure 6. Movement of slope surface (Slope-I-2)

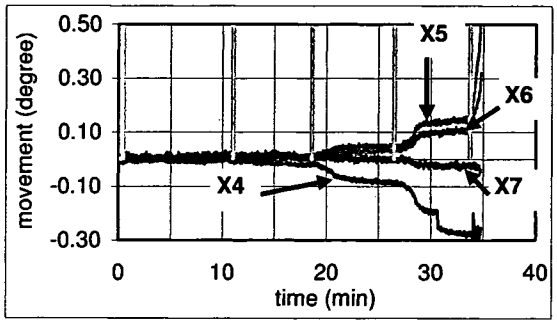

Figure 9(b). Tilt sensors on slope top (Slope-I-2)

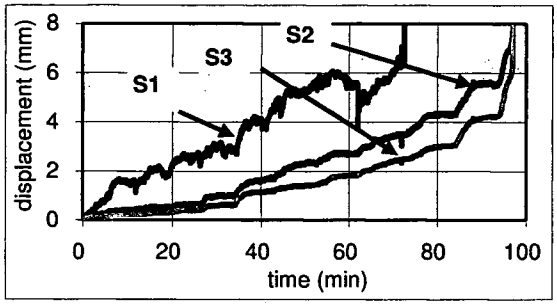

Figure 7. Movement of slope surface (Slope-IV-1)

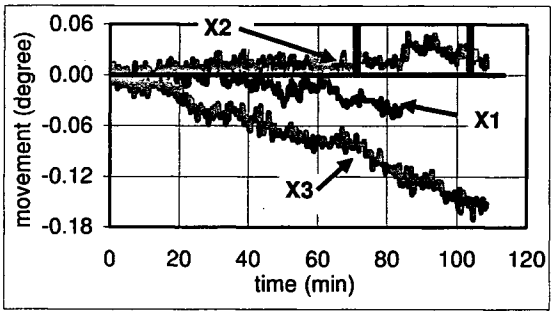

Figure 10. Tilt sensors on slope surface (Slope-IV-1)

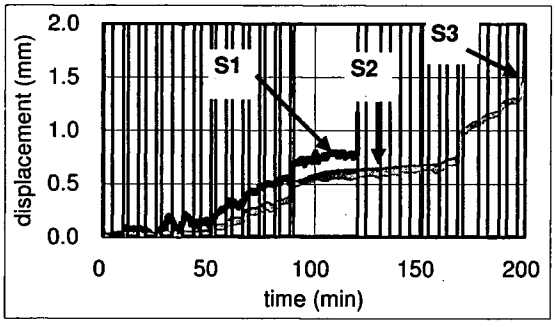

Figure 8. Movement of slope surface (Slope-V-1)

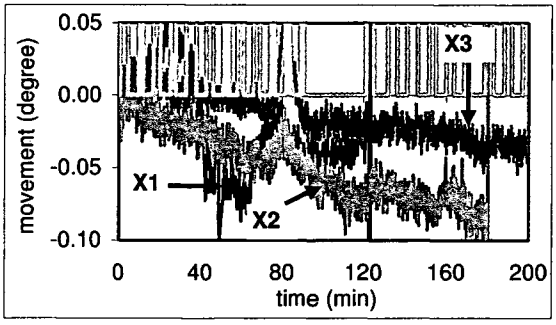

Figure 11(a). Tilt sensors on slope surface (Slope-V-1)

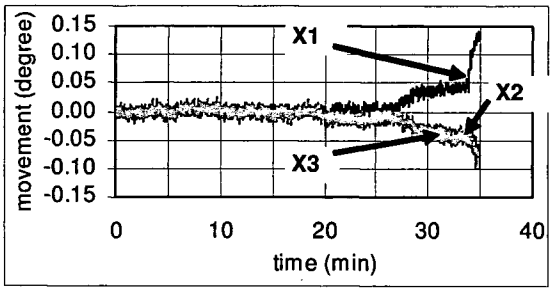

Figure 9(a). Tilt sensors on slope surface (Slope-I-2)

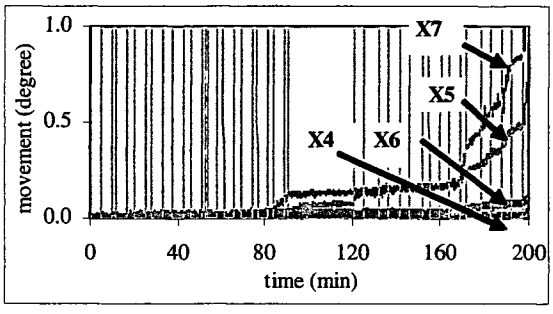

Figure 11(b). Tilt sensors on slope top (Slope-V-1)

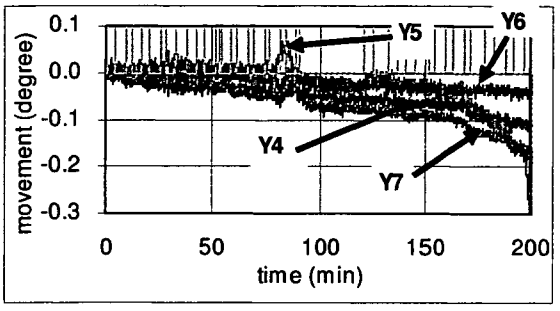

Figure 11(c). Tilt sensors on slope top (Slope-V-1)

3.2 Centrifuge Test Results

In Figs. 12, relationship between elapsed time and vertical displacement of slope top measured by LVDTs are shown. Failure step and elapsed time of failure are shown in Table 2. In all the test cases, vertical deformation increases with the increase in excavation steps. Except for case 60A (Fig. 12(c)), gradual increment in the vertical deformation; specially LVDT-1 and LVDT-2 just before the failure was seen for all the cases. Large and sharp increment in vertical deformation was seen for the cases of 50B and 60B which have larger slope height. Small or sudden failure was seen for slopes having smaller slope height (50A, 60A and 70A cases). Also, elapsed time to failure for slopes having higher slope height is longer than slopes having smaller slope height.

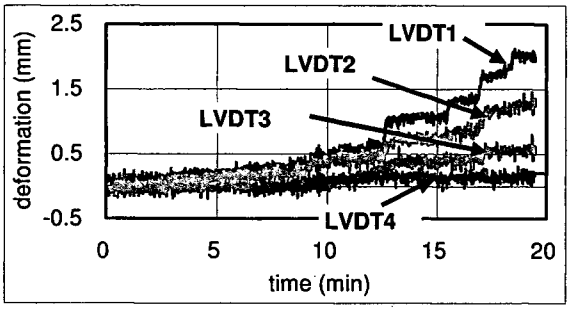

Figure 12(a). Deformation on slope top (50A)

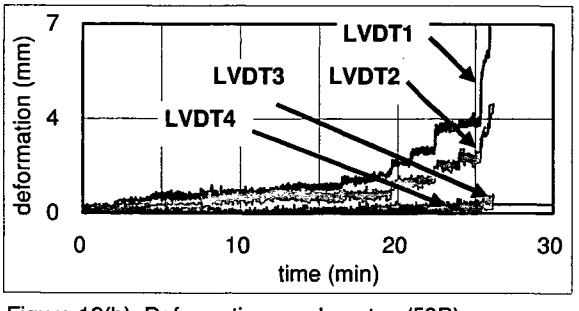

Figure 12(b). Deformation on slope top (50B)

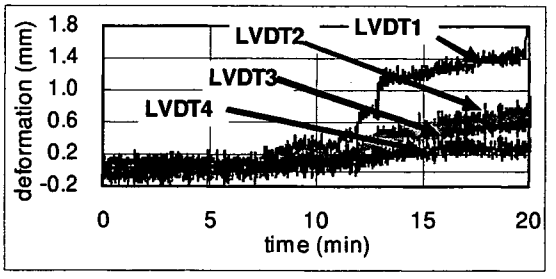

Figure 12(c). Deformation on slope top (60A)

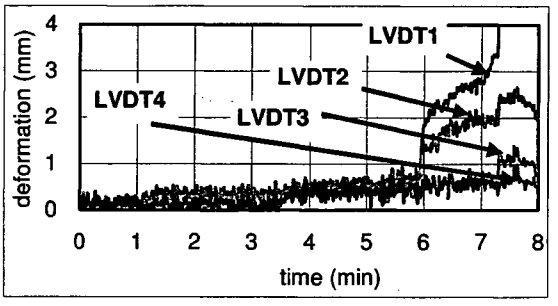

Figure 12(d). Deformation on slope top (60B)

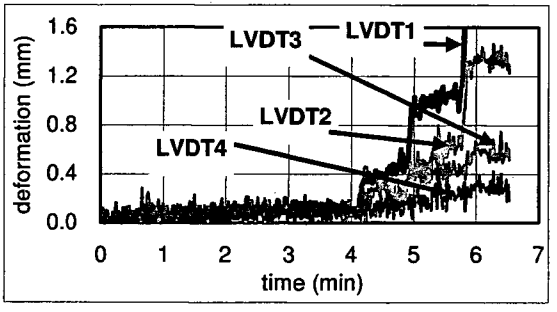

Figure 12(e). Deformation on slope top (70A)

Comparing the slope angles (50, 60 and 70 degrees), it was seen that the slopes having higher slope angle failed sooner than those having smaller slope angles. Number of excavation (steps) carried out up to failure also decreases with the increase in the angle of slope. Also, amount of deformation before the failure was larger for 50A than 60A and 70A, 70A showing the minimum value. Therefore, it could be said that slopes having higher slope angle and larger slope height fails sooner than those having smaller slope angle and smaller slope height. Similar results were seen in small scale full size tests also. This is due to weight of the slope behind the cut which increases with the increase in slope angle and slope height. More sharp increment in LVDTs was seen for 50B and 60B in comparison to 50A and 60A just before the failure. This means that for higher slopes, movement of slope is very faster and quicker than those for smaller height slopes. As

explained earlier, soil mass behind the excavation (cut) might have affected the movement of the slope.

3.3 Limit Equilibrium Analysis Results

Effective angle of cohesion and effective angle of frictional resistance measured from the direct shear test were 2.09 kPa and 37.22 degrees, respectively. These values were used in limit equilibrium analysis. Figure 13 shows the failure plane obtained from limit equilibrium analysis for 60A. Factor of safety (F.S.) obtained for all the tests are shown in Table 3. Slopes 50B, 60A, 60B and 70A were failed with F.S. value around 1.03 to 1.13. During the centrifuge test also, failure was occurred with the same amount of excavation. Factor of safety in case of 50A slope was around 1.26 to 1.28, showing the lesser possibility of complete failure. Partial failure was seen for 50A case during the centrifuge test also. Factor of safely around 1 obtained from limit equilibrium analysis showed that the centrifuge test results have good resemblance with the analysis data.

Figure 13. Failure plane from analysis (for 60A)

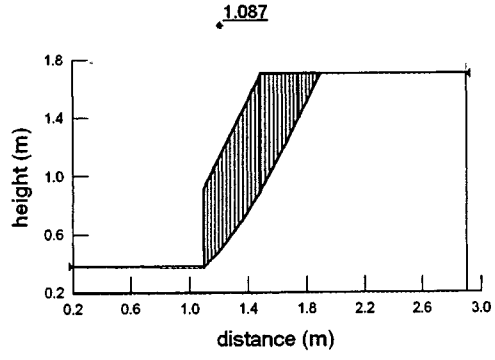

Table 3. Factor of safety from limit equilibrium analysis.

Method	50A	50B	60A	60B	70A
Ordinary	1.28	1.13	1.09	1.04	1.13
Bishop	1.26	1.13	1.08	1.03	1.12
M-P	1.27	1.13	1.09	1.03	1.13

5. CONCLUSIONS

From the small size full scale tests, following conclusions could be withdrawn;

1. With the step and time of excavation, movement of slope surface and deformations of the slope top could be measured from the start to the end of the excavation using laser sensors and vertical displacement transducers. Measurement of steep and sharp changes in the movement and deformation just before the failure showed the possibility of measurement of failure in advance.

2. Tilt-sensor also gave the gradual response with the time and step of excavation. Sharp and steep changes in the tilt angle both on the slope surface and slope top just before the failure was possible to measure. The trend of movement of tilt sensors is similar to the movement and deformation of laser sensor and vertical displacement transducers. This showed the possible application of tilt sensors in the excavation field for the prediction of failure in advance. With X and Y direction movements, possible direction of failure could also be predicted.

3. LVDTs used to measure the deformation of slope top in the centrifuge tests showed the graudual increment with elapsed time of excavation. Comparing the deformation amount of LVDTs on the centrifuge top, it was seen that the maximum movement was observed for the LVDTs set up at the nearest to the crest. This shows the possible position for the measurement of deformation

4. In both the small scale full size tests and centrifuge teste, slope having larger slope angle showed the quicker failure and smaller deformation in comparison to slopes which have small slope angle. Similarly, slopes with larger slope height showed shorter elapse time for failure than those with smaller slope height. Also, deformation pattern just before the failure for slopes having higher slope height are more steep and sharp than those for smaller height slopes.

5. Factor of safety obtained was around 1.03 to 1.13 except for 50A which is around 1.28. Since the analysis was carried for centrifuge model test just before the failure, it varifies that centrifuge test resutls are appropriate.

ACKNOWLEDGEMENT

This research is partially carried out under the Health and Labor Sciences Research Grants of Ministry of Health, Labor and Welfare. Authors are also thankful to Mr. Taiki Kasama of Hokkaido University for his help during centrifuge tests. Thanks are also extended for Akebono Brake Industries Co. Ltd., Tokyo for her support in preparing the tilt sensors.

References

Horii N., Itoh K, Toyosawa Y., and Tamate S. (2006) Development of the NIIS Mark-II Geotechnical Centrifuge, *International Conference on Physical Modelling in Geotechnics*, Hongkong (under print).

Toyosawa, Y., Horii, N., & Tamate, S. (1998) Deformation and failure behavior of anchored retaining wall induced by excessive excavation in centrifuge model tests, *Research Reports of the National Institute of Industrial Safety*, (NIIS-RR-97):35-46.

STABILITY OF TRENCH EXCAVATION UNDER CONSTRUCTION MACHINERY LOAD

Toyosawa Yasuo, National Institute of Industrial Safety, Tokyo, Japan
Yang Junjie, Ocean University of China, Qingdao, China
Timpong Sahaphol, National Institute of Industrial Safety, Tokyo, Japan
Itoh Kazuya, National Institute of Industrial Safety, Tokyo, Japan
Tamrakar Surendra Bahadur, National Institute of Industrial Safety, Tokyo, Japan

ABSTRACT
Trench collapse causes a considerable number of deaths and injuries of workers every year in Japan. In this paper, a series of centrifuge modelling was conducted in order to examine the stability of trench excavation under the construction machinery load. The NIIS in-flight excavator was used to simulate the trench excavation process during the centrifuge test. In addition, the effects of ground condition, magnitude and location of the construction machinery load on the failure mechanism were also investigated. The centrifuge test results clearly revealed that the mechanism of failure was mainly controlled by the magnitude of the machinery load and the bearing capacity of ground.

RÉSUMÉ
Les effondrements de tranchées engendrent un nombre considérable des morts et blessés chez les ouvriers tous les ans au Japon. En cette thèse, une série de modélisations centrifuges a été conduite afin d'examiner la stabilité de l'excavation de tranchée sous la charge des engins de construction. L'excavatrice embarquée NIIS a été utilisée pour simuler le processus d'excavation de tranchée pendant l'essai centrifuge. En outre, les effets de l'état au sol, de l'importance et de l'emplacement de la charge des engins de construction sur le mécanisme de rupture ont également été étudiés. Les résultats des essai centrifuges ont clairement montré que le mécanisme de rupture était principalement contrôlé par l'importance de la charge des engins et la portance du sol.

1. INTRODUCTION

There are many labor accidents in which the workers are killed and buried under collapsed ground when the construction machinery such as a drag shovel falls or topples over the edge of the trench during excavation. Photograph 1 shows the example of the ground collapse during the trench excavation. Based on the labor accident reports, during the period of 1994 to 2002, there were approximately 30 workers killed every year in Japan due to this type of failure. To prevent the loss of life and injury caused by the ground collapse, it is necessary to gain more understanding about the effect of construction machinery load, geometry of ground excavation (e.g. slope angle and excavation depth) and characteristic of ground strength on the stability of trench excavation. Geotechnical centrifuge modelling is commonly accepted as a powerful tool for studying a wide range of geotechnical problems. The stability and failure mechanism of ground excavations have been investigated using the centrifuge modelling by many researchers (Kusakabe 1982, Taylor 1984 and Toyosawa et al. 1994). However, the stability and failure mechanism of trench excavation under the construction machinery load have not been fully investigated. Therefore, in this paper, a series of centrifuge modelling tests was conducted on various types of ground models under different magnitudes and locations of the machinery load in order to examine the stability and the failure mechanism of trench excavation under the construction machinery load.

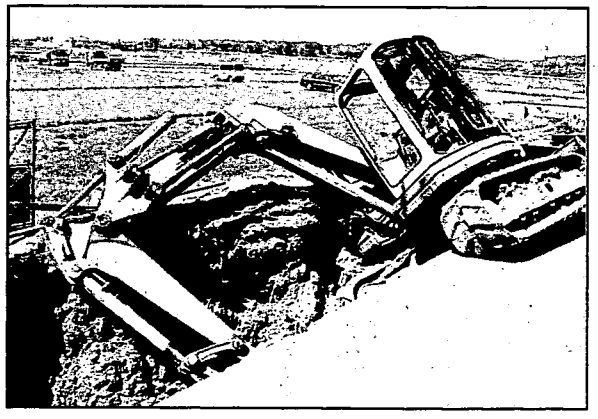

Photograph 1. Ground collapse during trench excavation

2. CENTRIFUGE MODELLING

In this paper, a series of centrifuge tests was performed using the Mark-II centrifuge in the centrifuge test laboratory of the National Institute of Industrial Safety (NIIS). The NIIS Mark-II centrifuge has an effective radius of about 2.3 m with a maximum acceleration of 100g and 50g under the static and dynamic conditions, respectively. The detail of the NIIS Mark-II centrifuge was described by Hori et al. (2006). The centrifuge tests were conducted on ground models at the centrifuge acceleration of 30g and test results were presented in the model scale.

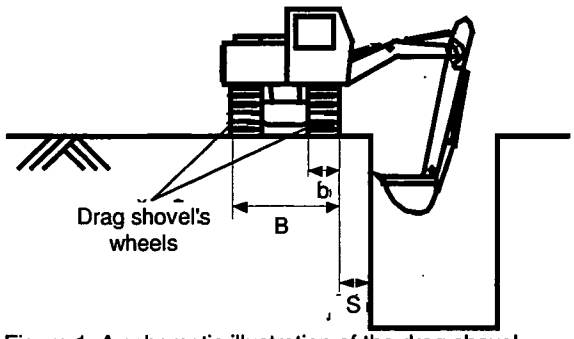

Figure 1. A schematic illustration of the drag shovel

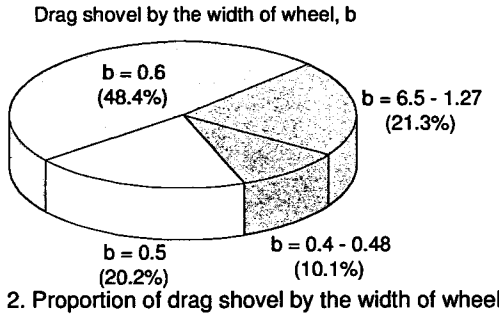

Figure 2. Proportion of drag shovel by the width of wheel

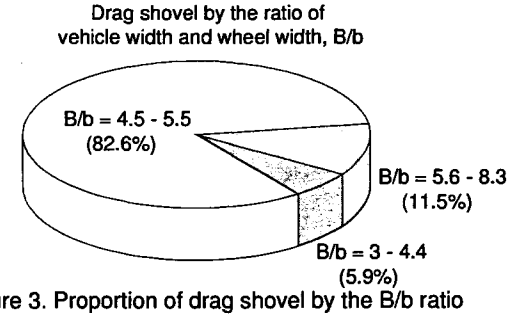

Figure 3. Proportion of drag shovel by the B/b ratio

2.1 Modelling of Construction Machinery Load

Figure 1 shows a schematic illustration of the drag shovel which is commonly used in trench excavation, the geometry of the drag shovel such as a full width of vehicle or crawler (B), a width of wheel (b) and a side clearance from the slope crest (S) are also presented in the figure. Based on the investigation of 287 different types of the drag shovels used in the trench excavation, the specifications of the drag shovel including the vehicle width, the width of wheel and the bearing pressure of the wheel can be characterized as shown in Figures 2 and 3. The bearing pressure of wheel or crawler is in the range of 9.8 to118 kPa. Figure 2 shows the proportion of the drag shovel by the width of wheel, b. It was found that the width of wheel distributes in the range of 0.4 to 1.27 m and approximately 50% of the drag shovels have the width of wheel of 0.6 m. Figure 3 shows the proportion of the drag shovel by a ratio of the vehicle width and the width of wheel, B/b. As can be seen in the figure, about 83 % of the drag shovels have the vehicle width of about 5 times of the width of wheel. Therefore, in this paper, the construction machinery load was modelled by a rigid block (U-shape) with b = 0.6 m (in prototype scale) and B/b = 5 as shown in Figure 4. It should be noted that the machinery load was modelled under the static condition.

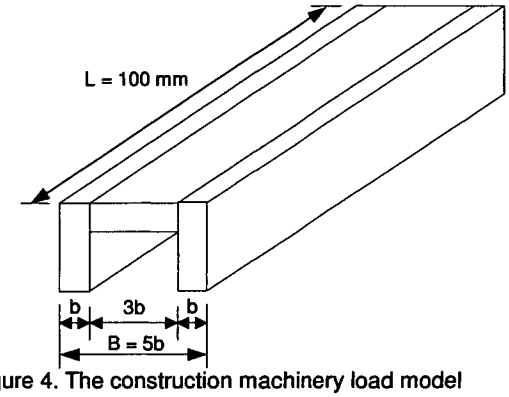

Figure 4. The construction machinery load model

2.2 Ground Model Preparation

The ground model was prepared in a rigid model box (internal dimensions of 100 mm in width, 450 mm in length and 272 mm in height) with a transparent Plexiglas front wall in order to provide side viewing of the ground model during the centrifuge test. The membrane was attached onto the ground model and silicone grease was smeared between the sidewall of model box and the membrane to reduce the sidewall friction. Three different kinds of ground models were prepared, namely, uniform sand ground model (model A), layered sand ground model (model B) and Kanto loam (a volcanic cohesive soil in Japan) ground model, (model C). The preparations of the ground models are described as follow.

Ground model A: the uniform sand ground model was prepared by pluviating air-dried Toyoura sand from a sand hopper through air at a controlled drop height into the rigid model box. Toyoura sand is classified as a uniform clean fine sand with a mean grain size, D_{50} = 0.18 mm and a density of soil particle, ρ_s = 2.65 g/cm^3. By this method, homogeneous dense sand ground model with a relative density, D_r of about 78% was obtained. The ground model was saturated by soaking the ground model in the water for about 24 hours. After the saturation process, the water content, w of the ground model of 21.6 % was obtained. In order to examine the degree of saturation, S and the water content of the ground model at the centrifuge test condition (at acceleration of 30g), the ground model was placed onto the centrifuge swinging platform and the centrifuge acceleration was gradually increased to the acceleration of 30g. It was found that the degree of saturation and the water content decreased with time and the water content and the degree of saturation remained unchanged after 15

minutes (w = 3.2%, S = 15.2%). The density of the ground model was about 1.620 g/cm^3. After the centrifuge test, the water content was measured at every 5 cm depth from the ground surface and uniform value of the water content was observed.

Ground model B: the layered sand ground model was prepared by the same material and method as used in the ground model A. However, after pluviating Toyoura sand into the model box to a thickness of approximately 10 mm, the pouring hole of the sand hopper was closed. The ground surface was levelled and the colored-dyed Toyoura sand was then placed on the ground surface with a thickness of about 5 mm in order to highlight the deformation and the location of failure surface. Thereafter, the pouring hole was reopened and the next ground layer was prepared using the same method described above. The water content and the degree of saturation of the ground model were consistent well with that of the ground model A, and the density of the layered sand ground model after the test was about 1.605 g/cm^3.

Ground model C: the Kanto loam with the particle size passing the 2 mm sieve was used in this ground model. The water was sprayed and mixed with the Kanto loam to provide the conditions of optimum water content in advance. The ground model was placed into the model box and compacted under a pressure of 49 kPa by the bellofram cylinder. For the first ground layer with a thickness of about 70 mm, the Kanto loam of 2500 g was compacted for 30 minutes. For the next ground layers, the Kanto loam was compacted in layer of about 7.5 mm thick for a total of 18 layers. After each compaction, a thin layer of air-dried kaolin powder was placed on the ground surface for the observation of the failure surface. By this method, the relative density, the wet density, and the water content of the ground model were about 66 %, 119% and 0.928 g/cm^3, respectively. After completion of the preparation of ground models, the construction machinery load model was then placed on the top of the ground surface at the specific location. The typical experimental model is shown in Figure 5.

2.3 Characteristics of Ground Models

In order to evaluate the strength of the ground models, the small-sized cone penetration test and the bearing capacity tests were conducted in the centrifuge test. The small-sized cone penetrometer has a diameter of 5 mm with a base area and a tip angle of 0.196 cm^2 and 60 degrees, respectively. Figure 6 shows the cone penetration test results for the ground model A, B and C, the cone resistance increased linearly with depth and centrifuge acceleration level for the uniform sand (model A) and the layered sand (model B) ground models. It should be noted that the test result was presented corresponding to the model scale. As expected, the ground model B has a lower cone resistance than that of the ground model A for a given centrifuge acceleration. This is mainly due to the weakness of the colored sand layers. In contrast, in case of Kanto loam ground model (model C), the uniform ground strength can be observed in which slope of the cone resistance-depth curve drop at the depth of about 20 mm and the cone resistance remains unchanged with depth. In addition, the cone resistance of the ground model under the 1g gravity field and the centrifuge acceleration of 30g are almost identical.

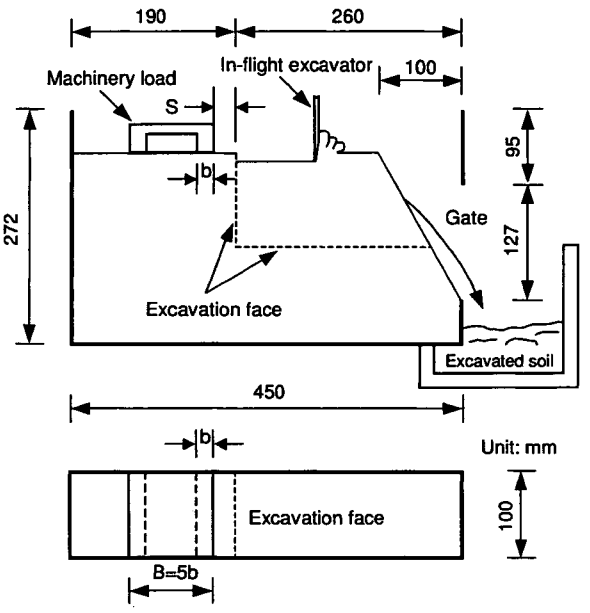

Figure 5. Typical experimental model setup

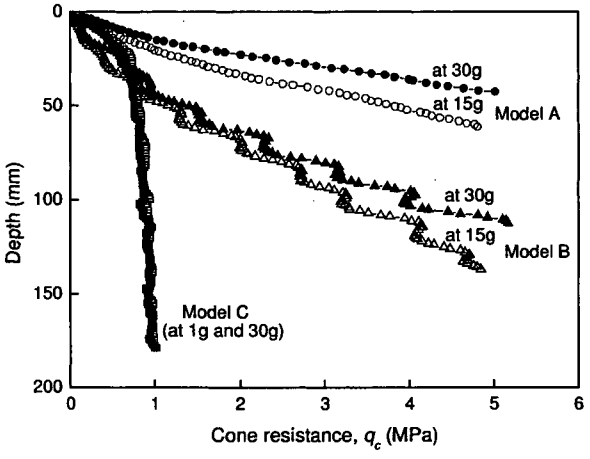

Figure 6. The cone penetration test results

This behavior may be attributed to the fact that the overburden pressure due to the self-weight of ground at the acceleration of 30g is lower than that of the preconsolidation pressure of 49 kPa, therefore, the effect of the acceleration level seems to be insignificant. The bearing capacity tests with a footing model of 20 mm in width (Bm) were conducted at the centrifuge acceleration

of 30g. The test results for the ground model A, B and C are presented in Figure 7, the bearing capacity, q is plotted with the normalized settlement, S_m / B_m. As can be seen in the figure, the ultimate bearing capacity of 1230 kPa and 700 kPa are observed in the ground model A and B, respectively. It is obvious that the ground model C has the lowest ultimate bearing capacity (91 kPa) when compare with the other ground models.

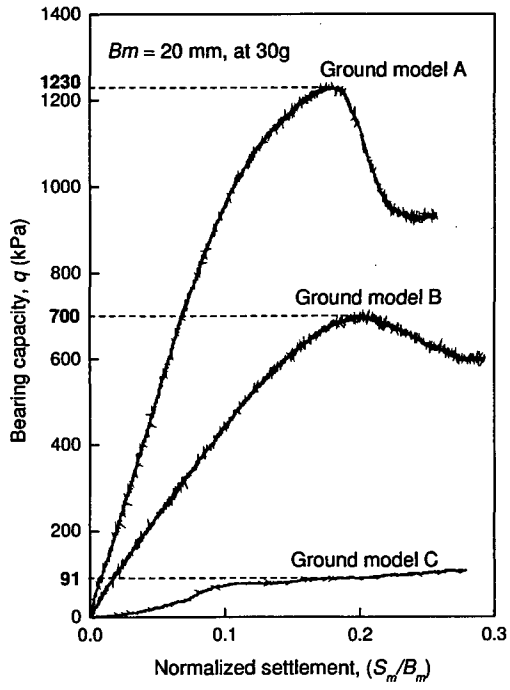

Figure 7. The bearing capacity test results

2.4 Test Conditions

A series of centrifuge tests was conducted on the three different ground models under different magnitudes and locations of the construction machinery load. The test conditions are summarized in Table 1. In addition, the centrifuge tests were also conducted on the ground models without the machinery load for the comparison.

Table 1. Summary of the test conditions

Ground model	b (mm)	Bearing pressure (kPa)	S/b
A	20	35.4	0.5,0.75,1.25,1.75
B	20	35.4	0.5,0.75,1.25,1.75
C1	20	35.4	1.25
C2	20	91.7	0.5,0.75,1.25,1.75

As can be seen in the Figure 7 and the Table 1, the bearing pressure of the machinery load (35.4 kPa) is small very about 3% and 5% of the ultimate bearing capacity of the ground model A and B, respectively. While in the ground model C1, the bearing pressure of the machinery load is about 40% of the ultimate bearing capacity. In order to see more clearly the influence of the bearing pressure on the stability of trench excavation, the machinery load model with the bearing pressure of about the same as the ultimate bearing capacity of ground was used in the model C2.

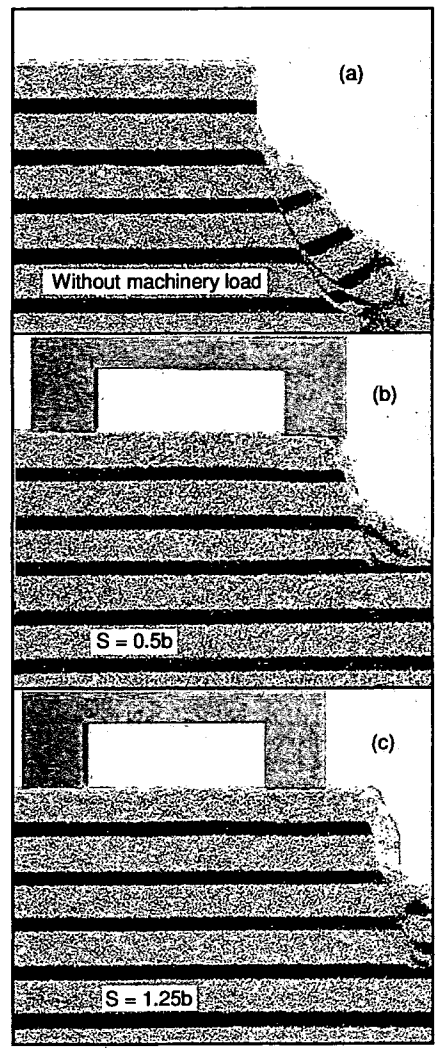

Photograph 2. Ground model B after failure, (a) without machinery load, (b) with machinery load S = 0.5b and (c) with machinery load S = 1.25b

2.5 Test Procedures

After completion of the experimental model setup, the ground model was loaded onto the centrifuge swinging platform and the centrifuge acceleration was then increased gradually until the acceleration of 30g. The NIIS in-flight excavator (Toyosawa et al. 1998), which is

capable of excavating the ground model during the high centrifuge acceleration environment was used in this paper for simulating the trench excavation process. After the centrifuge acceleration reached 30g, the ground model was excavated vertically with a thickness of about 5 mm until the ground failure can be observed. The excavation depth at just before the ground failure was recorded and defined as the maximum excavation depth.

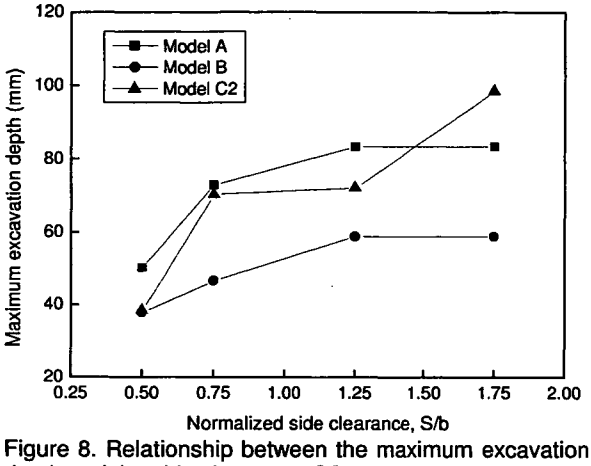

Figure 8. Relationship between the maximum excavation depth and the side clearance, S/b

3. EXPERIMENTAL RESULTS

3.1 Failure Mechanism of Sand Ground

Photograph 2(a) shows the cross-section of the ground model B after the failure in case of no machinery load, and photographs 2(b) and (c) are the example of the failure pattern of the ground model B under the machinery load. The failure pattern of ground model A is identical with that of the ground model B even the photographs are omitted here. It is obvious from the photographs that the failure mechanism is mainly due to the instability of slope. This may be attributed to the fact that in case of the sand ground models (models A and B) the bearing pressure of the machinery load is relatively small when compare to the ultimate bearing capacity of ground. Therefore, the self-weight of ground plays the important role on the instability of slope.

Figure 8 shows the relationship between the maximum excavation depth and the normalized side clearance, S/b of the ground model A, B and C2. The maximum excavation depths of the ground model A and B in case of no machinery load are 83 mm and 58 mm, respectively. It is apparent that the maximum excavation depth increases with the side clearance in the ground model A and B. However, when the side clearance is more than 1.25b, the influence of the side clearance on the maximum excavation depth seems to be insignificant in which the maximum excavation depth under the machinery load is almost the same as in case of no machinery load.

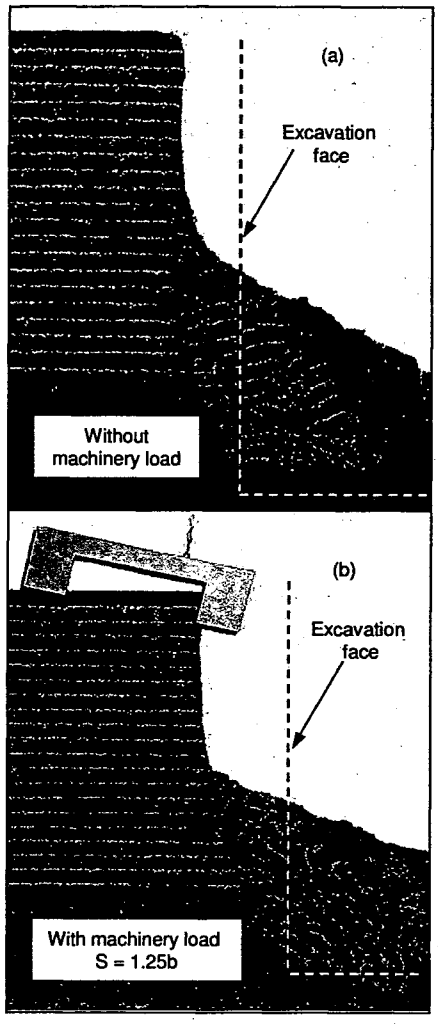

Photograph 3. Ground model C1 after failure, (a) without machinery load and (b) with machinery load S = 1.25b

3.2 Failure Mechanism of Kanto Loam Ground

Photograph 3(a) shows the failure pattern of the ground model C1 in case of no machinery load. The maximum excavation depth of about 220 mm was observed after the failure. Photograph 3(b) shows the failure pattern of the ground model C1 under the machinery load. The bearing pressure of the machinery load is about 40% of the ultimate bearing capacity of ground. The machinery load model was hung with the iron wire in order to prevent the damage of the failure pattern due to the falling of machinery load model after the failure. The maximum excavation depth of about 180 mm was observed at S = 1.25b. By comparing the photographs 3(a) and (b) the failure patterns of the ground model C1 with and without the machinery load are almost identical. In addition, the mechanism of failure is similar to that of the sand ground models in which the instability of slope is a major cause of failure. On the other hand, in case of ground excavation under the machinery load with the bearing

pressure equal to the ultimate bearing capacity of ground (model C2), the failure mechanism is totally different as can be observed in Photographs 4(a), (b) and (c).

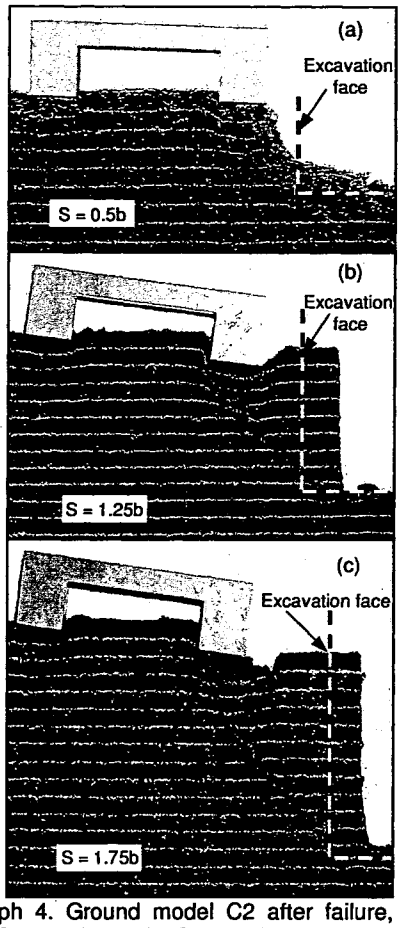

Photograph 4. Ground model C2 after failure, (a) S = 0.5b, (b) S = 1.25b and (c) S = 1.75b

Figure 9 shows the schematic illustrations of the failure mechanism observed in the ground model C2. The failure mechanism was initiated by the collapse of ground beneath the machinery load due to the insufficient of ground bearing capacity, and the surrounding ground was then pushed towards the excavation face. It was considered that the failure mechanism was similar to the bearing capacity failure of foundation. The increase in the maximum excavation depth with the side clearance of the ground model C2 can be observed in the Figure 8.

It should be noted that at the side clearance of 1.75b, the maximum excavation depth is only about 50% of that observed in case of no machinery load (maximum excavation depth of 220 mm). This indicates that the influcenece of the side clearance on the maximum excavation depth is more significant in the ground model C2 than the ground model A and B.

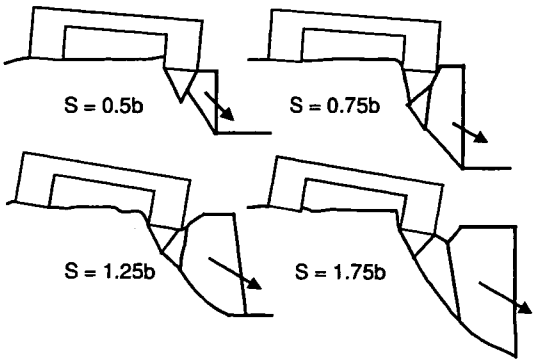

Figure 9. The failure mechanism of the ground model C2

4. CONCLUSIONS

The size and magnitude of the construction machinery load were modelled according to the investigation of drag shovel specifications. The failure mechanisms of trench excavation under the construction machinery load are different depending on the magnitude of bearing pressure of the machinery load and the ultimate bearing capacity of ground. When the bearing pressure of the machinery load was smaller than the ultimate bearing capacity of ground, the failure mechanism was mainly due to the instability of slope. On the other hand, when the bearing pressure was approximately equal to the bearing capacity of ground, the failure mechanism was similarly to the bearing capacity failure of foundation and the effect of the side clearance on the maximum excavation depth was highly significant. In addition, because the construction machinery usually operates under the dynamic condition, further research should be conducted to examine the stability of trench excavation under the dynamic load.

References

Horii, N., Itoh, K., Toyosawa, Y. and Tamate, S. (2006) Development of the NIIS Mark-II geotechnical centrifuge, *International Conference on Physical Modelling on Geotechnique, Hong Kong.* (in press)

Kusakabe, O. (1982) Stability of excavations in soft clay, *Ph.D thesis*, Cambridge University.

Taylor, R.N. (1984) Ground movements associated with tunnels and trenches, *Ph.D thesis*, Cambridge University.

Toyosawa, Y., Horii, N., Tamate, S., Hanayasu, S. and Ampadu, S.K. (1994) Deformation and failure characteristics of vertical cuts and excavations in clay, *Proceeding of International Conference on Centrifuge 94, Singapore*: 663-668.

Toyosawa, Y., Horii, N., and Tamate, S. (1998) Deformation and failure behavior of anchored retaining wall induced by excessive excavation in centrifuge model tests. *NIIS Research report*, NIIS-RR-97: 35-46.

Comparison of Failure Mechanism due to Toe Excavation: Field test, Centrifuge test and Numerical Analysis

S B Tamrakar, Japan National Institute of Occupational Safety and Health, Tokyo, Japan
Y Toyosawa, Japan National Institute of Occupational Safety and Health, Tokyo, Japan
K Itoh, Japan National Institute of Occupational Safety and Health, Tokyo, Japan
T Mitachi, Graduate school of Engineering, Hokkaido University, Hokkaido, Japan

Abstract

To understand the failure mechanism and vertical deformation behavior during the failure of slopes due to excavation, two embankment slopes were prepared in the field from Narita sand (NS) by compaction with bull dozer. Degree of compaction was varied; loose compaction (NSL) and high compaction (NSH). Toe excavation for these embankments were continued until failure occurred by back hoe. Measurement of deformation of the slope top was carried out using invar extensometer and laser beam-optical sensor. These field embankments were modeled in the centrifuge, and in-flight excavator was used to cut the toe of the slopes until failure occurred. Linear vertical differential transducers (LVDTs) were set up on the slope top in the centrifuge model to measure the vertical displacement of slope top. Similarly, numerical analyses were carried out for the field embankments. From numerical analysis, in case of NSL, failure was occurred due to increase in the zone of plastic points from the toe of the slope towards the slope top. Also, zone of plastic points were appeared and increased on the slope top. These zones of plastic points later on combined and final failure occurred. In case of NSH, failure was observed due to increment of plastic zone at the toe and tension cut off zone at the slope top, separately. Accordingly failure pattern in the field for NSL and NSL were different. Finally, vertical displacement was compared. Although some differences in their amount were seen, the displacement pattern after 4^{th} excavation was similar for all the cases.

Keywords: Toe excavation, centrifuge, numerical analysis, PLAXIS, embankment

Introduction

Slope failures are occurred either due to natural phenomenon such as heavy rain or earthquakes or due to human construction works such as slope cutting or excavation or embankment. Failure of slope due to natural phenomenon is unavoidable. But those occurred due to human construction works could be reduced to some extent. Slope failure accidents occurred due to human construction works sometimes takes the lives of the worker and damage the properties around. As shown in Fig. 1,

in Japan accidents (death) due to construction works are reducing every year. In comparison to this, the death accidents those are occurred due to slope failures are not reducing. Every year, about 30 to 40 cases of accidents due to slope failure are recorded. To protect the unstable slope, either retaining wall is constructed or slope is cut to more stable slope angle. But in either case, slope has to be cut. During this cutting or leveling the trench for retaining wall at the toe of the slope, slopes are at the greater risk of failure. In many cases, without any prior signals of failure, sliding occurs instantaneously. Slopes become safe only when the cutting is reached to safer slope or retaining wall construction is completed. More than 50% of slope failure accidents are occurred during cutting or leveling the trench of lower part of the slope.

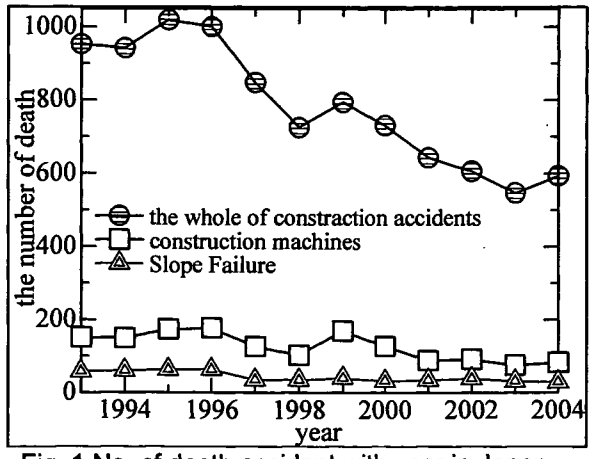

Fig. 1 No. of death accident with year in Japan.

Earlier, Tamrakar et al. (2005 and 2006) had discussed about the failure slope height during the excavation of volcanic sand, Kanto loam and mixture of NSF clay and Toyoura sand slopes. For this, they had performed in-flight excavation in the centrifuge environment and discussed about the difference in the slope failure height while making toe excavation with and without trench excavation at the beginning. Saito et al. (2002), Tamrakar et al (2006), Tamate et al. (2006) and Itoh et al. (2006) had discussed about the methods and instrument of measuring the movement of failure trend just before the failure during excavation in the field. Here, to understand the failure mechanism during field excavation, slope excavation was made at the field and toe excavation was carried out until failure. Then centrifuge in-flight excavation and numerical analyses were carried out for the field embankments so that the failure mechanism and deformation of slope top during the excavation could be made.

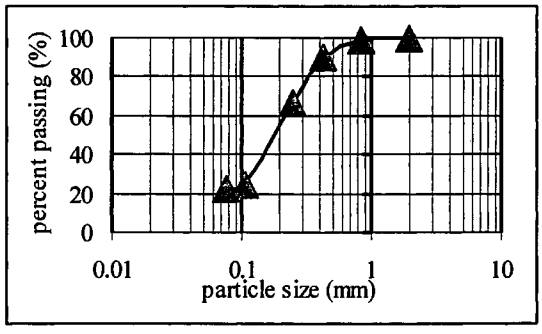

Fig. 2. Grain size distribution curve.

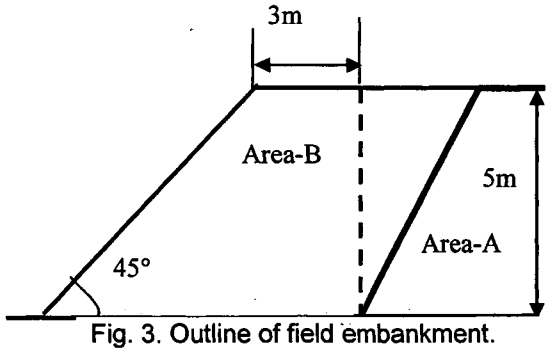

Fig. 3. Outline of field embankment.

1. Field embankments

In the field, four embankments were prepared at Toke (Housing construction site) of Chiba prefecture, Japan (Horii et al. 2006). Here, the two embankments made with Narita sand (NS) are only explained. Narita sand was obtained from the same construction site. Grain size distribution curve is shown in Fig. 2. This soil is classified as SP-G and its soil density (ρ_s) is 2.76 g/cm^3. Embankments were prepared by compacting the soil in layers with the help of a bull dozer (7 tons). Degree of compaction was varied for two types of embankments; lightly compacted one is called NSL and highly compacted one is called NSH. Outline of embankments is shown in Fig. 3. Area A in the figure shows the natural cut while area B shows the embankment constructed. Slope angle is 45° and slope height is 5m with 3.5m width. Photo 1 shows the completed embankments.

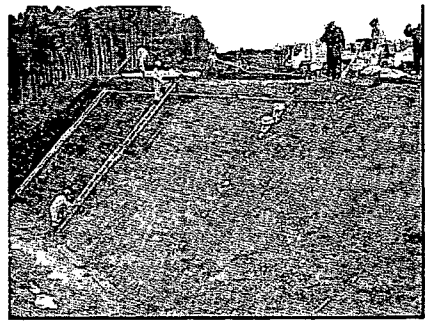
Photo. 1. Field embankment.

For the measurement of the movement of slope top (crest), one invar wire extensometer and a set of laser beam-optical sensor were set up. They were set up at 0.5 m distance from the crest of the embankment. Invar wire extensometer is a commonly used instrument in the field for the